Resonance EMAT system for acoustoelastic stress measurement in sheet metals

M. Hirao, H. Ogi, and H. Fukuoka

Citation: Rev. Sci. Instrum. **64**, 3198 (1993); doi: 10.1063/1.1144328
View online: http://dx.doi.org/10.1063/1.1144328
View Table of Contents: http://rsi.aip.org/resource/1/RSINAK/v64/i11
Published by the American Institute of Physics.

Resonance EMAT system for acoustoelastic stress measurement in sheet metals

M. Hirao, H. Ogi, and H. Fukuoka
Faculty of Engineering Science, Osaka University, Toyonaka, Osaka 560, Japan

(Received 14 May 1993; accepted for publication 17 August 1993)

A practical method of acoustoelastic stress measurement based on electromagnetic acoustic resonance is presented. This overcomes fundamental limitations of conventional procedures and exhibits the stress resolution to 0.1 MPa for thin aluminum plates and the spatial resolution to several millimeter square in a noncontacting operation. The proposed method successfully combines an electromagnetic acoustic transducer (EMAT) and a superheterodyne phase-sensitive detector. An EMAT is excited by a high-power rf burst in the 0.5–20-MHz range and generates ultrasonic oscillations in a plate through a Lorentz force mechanism. The signals in the plate are then received by this same EMAT and analyzed for the *amplitude spectrum* using swept-frequency phase-sensitive detection circuitry. The resonance frequencies can be determined for longitudinal and shear modes simultaneously. To illustrate the resonance spectrum technique, experimental results are shown for the measurement of a two-dimensional stress field in a thin aluminum plate. Liftoff sensitivity is also determined.

I. INTRODUCTION

Acoustoelasticity uses the stress dependence of ultrasonic velocities in solid bodies and provides a unique means for nondestructive stress determination.[1] Time-of-flight measurements for reflection echoes detect the interior stress averaged along the propagation path. While many other techniques are available to evaluate the surface stresses, the alternative to acoustoelasticity is only the neutron diffraction method, which is rarely accessible. Many instances of the successful industrial and field applications are emerging such as those for welded parts, railroad wheels, rails, bolts, and water pipes.[2–5] However, the wide acceptance of acoustoelasticity as a standard technique has been limited for several reasons. They include the high accuracy needed to cope with the low sensitivity to stress, the prolonged preparation, etc. It needs a high grade of surface finishing to assure the thinnest coupling layer between the piezoelectric transducer and the object surface, thereby achieving the required accuracy of velocity determination. Experimental difficulties arise when the path length is not long enough as will be encountered with the thin-walled structures like aircraft and fuel-storage vessels. The relative accuracy decreases with decreasing thickness. Eventually, the successive echoes are overlapping each other even if high-frequency, broadband signals are employed.

The resonance method is commonly adopted to determine the ultrasonic velocities and elastic constants of small samples (sphere, rod, sheet, etc.), although restricted to laboratory studies at present. In the present study, the electromagnetic acoustic transducers (EMATs)[6–8] are incorporated in the pulsed ultrasonic resonance spectrometer for acoustoelastic stress measurements. Besides the possibility of measuring thin plate geometries, new advantages result from using EMATs as generators and receivers. Because the EMATs operate using electromagnetic forcing mechanisms, they can generate and detect ultrasonic waves without an intimate contact with the testing object. This feature allows a liftoff (air gap) of several millimeters. Use of EMATs can avoid the corrections for the frequency shift which occurs with contacting transducers,[9–11] and also accommodates unprepared, even rusty and roughened, surfaces. This is attractive in many practical applications. In addition, driving the object into resonance most effectively makes up for the large insertion loss inherent in the EMATs, typically being 40 dB lower than using piezoelectric transducers. Following the excitation with long rf bursts to generate ultrasonics in the plate, the EMAT receives the multiple reflection echoes overlapping each other. Echoes have the amplitudes which decay exponentially with time and the phases which arise on the transduction and during the propagation in the plate. They are received all in phase exclusively at a resonance frequency to give a pronounced amplitude of ultrasonic ringing. Above and below the resonance frequency, the echoes interfere destructively, resulting in a faint amplitude. Their clear contrast works beneficially in producing a sharp resonance peak and results in a high velocity resolution. Finally, a wider frequency range is available with EMATs than PZT transducers, in general.

In the literature, Filimonov *et al.*[12] and Nikiforenko *et al.*[13] first implemented the resonance EMAT and observed the resonance peaks at two adjacent frequencies, for which an aspect of the material's elastic anisotropy, represented by B_0 (defined later), was responsible. Kawashima[14] has developed the resonance EMAT, up to 50 MHz, to measure the three velocities of longitudinal and polarized shear waves in steel sheets for estimating a texture parameter. Johnson *et al.*[15] used the EMAT approach to determine the resonance frequencies in small metal spheres. Acoustoelasticity needs a higher accuracy in

 0034-6748/93/64(11)/3198/8/$6.00

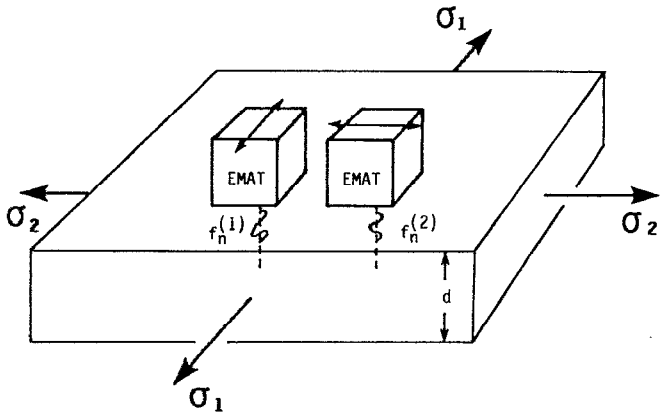

FIG. 1. Principle of birefringence stress measurement using a polarized shear-wave EMAT.

resonance frequency determination than the previous work. Kawashima has claimed the accuracy in the order of 10^{-4}. Stress detection to the 1-MPa resolution is possible only with the 10^{-5} relative accuracy or more in the velocity measurements for common metals.[1]

II. ACOUSTOELASTICITY WITH RESONANCE METHOD

Acoustoelastic theory establishes the linear dependence of elastic wave velocities on stresses on the basis of nonlinear elasticity, considering up to the third-order elastic constants.[1] Ultrasonic experiments support the theory with calibrated constants. It is straightforward to convert the acoustoelastic relations in terms of the propagation velocities into those in the resonance frequencies. In the case of a plate sample with the parallel, stress-free surfaces, the acoustic resonance (thickness oscillation) occurs at the frequencies defined by $f_n=nV/2d$, where V is the longitudinal or shear-wave velocity, d the plate thickness, and n an integer, indicating the order of resonant modes. The plate is an integer number of half-wavelengths thick. The sensitivity to stress increases as n increases. This implies that the transit time changes more as the number of reflection increases, responding to stress application.

The thickness can be eliminated by considering the ratios of resonance frequencies. Fractional velocity difference of shear waves having the polarization directions in the principal directions of stress, called acoustic birefringence B, is written as

$$B=\frac{f_n^{(1)}-f_n^{(2)}}{(f_n^{(1)}+f_n^{(2)})/2}=B_0+C_A(\sigma_1-\sigma_2), \tag{1}$$

where $f_n^{(1)}$ and $f_n^{(2)}$ are the nth resonance frequencies for the polarization in the principal stresses σ_1 and σ_2 (Fig. 1). The ratio of longitudinal wave velocity to the average of two shear wave velocities, denoted by R, is proportional to the sum of the principal stresses. This is expressed in terms of the resonance frequencies including $f_m^{(3)}$ for a longitudinal mode as

$$R=\frac{n}{m}\frac{f_m^{(3)}}{(f_n^{(1)}+f_n^{(2)})/2}=R_0+C_R(\sigma_1+\sigma_2). \tag{2}$$

The acoustoelastic constants C_A and C_R represent the sensitivity to stress, depending on the second- and third-order elastic constants. Although they show a weak dependence on material microstructures, it is the usual procedure to calibrate them in uniaxial loading tests ($\sigma_2=0$). The offsets B_0 and R_0 are observed at the stress-free state. When the material has no texture and is macroscopically isotropic, B_0 vanishes and R_0 takes the value of $\sqrt{(\lambda+2\mu)/\mu}$, where λ and μ are the second-order elastic constants. When B_0 and R_0 are both accessible in some way, we can determine the individual stresses by measuring B and R.

III. EXPERIMENTAL METHOD

A. Electromagnetic acoustic transducers (EMATs)

An EMAT is composed of permanent magnet(s) and a flat coil. Being placed close to a conducting object and activated by an rf burst signal, the coil induces an eddy current in the surface skin. The magnet applies a static magnetic field, which interacts with the induced current to create the Lorentz force. This body force is the source of mechanical vibrations, which radiate into the bulk of material. On reception, the reversed process takes place under the same EMAT. The mechanical motion associated with the elastic wave interacts with the magnetic field to cause the eddy current within the conductor's surface skin, which is inductively picked up by the coil. A single EMAT can thus function as the transmitter and receiver. The signal intensity with the Lorentz force mechanism is proportional to (excitation current) × (magnetic flux density)^2.[6,7] The main advantage of using EMATs is the contactless coupling so that they allow a liftoff from the surface of the object. Since the wave source is established within the material, not in the transducer, the surface condition is not important to obtain an effective transduction. Presence of surface roughness, oxide, or dirt is equivalent to adding to the liftoff. Negligible loading by EMATs minimizes the energy extraction and the signal modification on repeated reflections, which may otherwise arise with the contacting transducers.

We built two types of compact EMATs with Nd–B–Fe permanent magnets and enameled copper wires of 0.2-mm diameter. Figure 2 illustrates the simplified geometries and the Lorentz force mechanism in both types. The coil turn was determined so as to make the apparent impedance to be 50 Ω at a prescribed frequency; the EMAT impedance is highly inductive with little resistance.[16] The coil dimension and the number of turns are decreased to have higher operating frequencies. There is a tradeoff between the signal strength and the spatial resolution. The whole structure was molded in an epoxy resin for a handling convenience.

Shown in Fig. 2(a) is the EMAT used to transmit and receive the polarized shear waves, for which an elongated spiral coil of eight turns was used. The active area was sized 5×4 mm^2. The available band was from 0.5 to 17 MHz. A pair of magnets, having the opposite magnetiza-

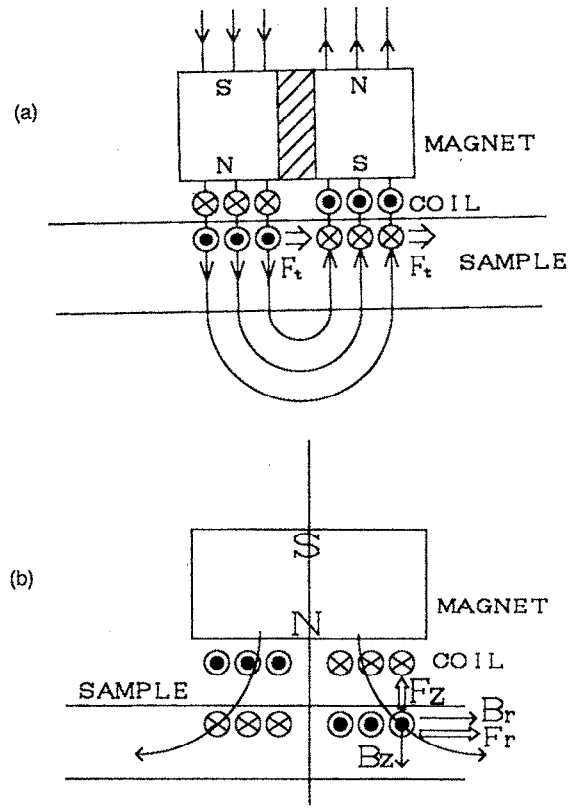

FIG. 2. Lorentz force mechanisms in shear-wave EMAT and dual-mode EMAT.

tion directions, were mounted on the straight sides of the coil with a spacer between them. A piece of steel bridged the top faces of the magnets to close the magnetic loop. This arrangement sets up a shearing force (F_t) perpendicular to the wire elements and parallel to the sample surfaces. This EMAT is rotated by 90° on the sample surface to measure $f_n^{(1)}$ and $f_n^{(2)}$ separately. For a moderately anisotropic material, due to stress and/or texture, double resonance peaks appear, when the EMAT is oriented near 45° from the principal directions; then, $f_n^{(1)}$ and $f_n^{(2)}$ are simultaneously measurable.

Dual-mode EMAT [Fig. 2(b)] consisted of a cylindrical magnet of 7-mm diameter and a pancake coil of 10-mm diameter. We wound the coil of seven turns with the double wires to electrically separate the transmitter and receiver portions and minimize the crosstalk between them. The resonance spectra were obtainable up to 12 MHz. Since the magnetic field "spreads out" axisymmetrically, the Lorentz force has the horizontal and vertical components as described by Kawashima.[14,17] The horizontal component (F_r) acts as the source for a radially polarized shear wave, which splits into two orthogonal polarizations and produces two resonance peaks in anisotropic samples. The vertical component (F_z) of the Lorentz force, which is dominant around the edging part of the magnet, excites the longitudinal wave. Poisson expansion/shrinkage accompanying the radial motion also induces the longitudinal wave from the central part. This effect occurs in a reversed phase relative to the direct Lorentz force excitation. With the dual-mode EMAT, a single measurement renders $f_n^{(1)}$, $f_n^{(2)}$, and $f_m^{(3)}$ at the same time in the presence of the acoustic birefringence. Since the longitudinal wave velocity is nearly twice larger than the shear-wave velocities, the longitudinal resonance is observed together with the shear resonance(s) of $n=2m$.

The dynamic magnetic field is also produced by the toneburst to the coil, being parallel to the sample surface. In the vicinity of the surface, this dynamic field interacts with the induced current to generate the longitudinal wave at twice the excitation frequency in both types of EMATs. However, the reversed process of this mechanism is incapable of detecting the longitudinal wave, because we do not apply the coil current in the receiving stage.

For the measurements in unfavorable conditions such as thick plates and lossy materials, we raise the rf voltage and the receiver gain and then the internal resonances of the EMAT become visible in the obtained spectra. This occurs because the magnets are conductors and the Lorentz reaction also generates elastic waves in them. We corrugated the top faces of the magnets to suppress these internal resonances as much as possible. They can be recognized in the spectrum measured without samples. We then selected the resonance peaks for stress measurements located far away from the internal resonances.

B. Superheterodyne phase-sensitive detector

Highly efficient and accurate determination of resonance frequencies was made possible by energizing the EMAT with long high-power rf bursts gated coherently. After the excitation ceases, the ultrasonic oscillation lasts with decaying amplitude, forming a ringing signal (reverberation) in the sample plate. A superheterodyne phase-sensitive detector acquires the amplitude and phase data by mixing and integrating the received ultrasonic signals with phase reference signals. Stepping the operation frequency F provides the spectroscopic data. Basically, the present instrumentation has a potential for measuring the amplitude and phase spectra, both with a high resolution needed for acoustoelasticity. Phase spectrum approach is useful to detect the stress-induced phase shift of an isolated reflection echo which travels a long distance, 20 cm for instance. This paper is, however, focused on the amplitude spectrum approach to utilize a train of heavily overlapped echoes for the pulsed resonance spectroscopy in thin plates. A detailed description of the functions and other applications of the superheterodyne phase-sensitive detector may be found elsewhere.[16,18–20] (The instrument is now commercially available from Ritec, Inc.)

Figure 3 presents the schematic block diagram of electronics. There are four multipliers playing central roles in the heterodyne processing. Multiplier No. 1 produces the cw at the operating frequency F for driving the EMAT using the signals from the IF oscillator and the synthesizer ($F+IF$); IF is the intermediate frequency fixed to 25 MHz. Multiplier No. 2 uses the synthesizer output to convert the frequency of the received ultrasonic signals into the bandwidth of the IF amplifier. This operation estab-

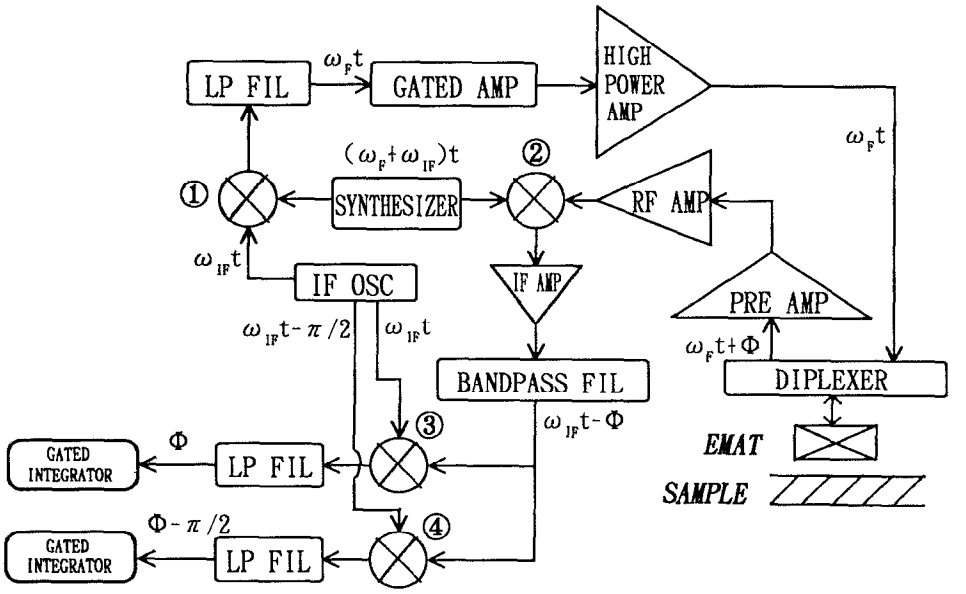

FIG. 3. Simplified block diagram of instrumentation for resonance EMAT, involving phases at various stages ($\omega_F=2\pi F$, $\omega_{IF}=2\pi IF$).

lishes the phase relationship between the transmitter and receiver subsystems and also removes the components other than the operating frequency F. In-phase and quadrature signals of the IF oscillator are fed to multiplier Nos. 3 and 4 to shift the frequency of the IF amplifier output to the dc range and extract the amplitude and phase of the ultrasonic signals. The components of sum frequencies are rejected by the low-pass filters following multiplier Nos. 1, 3, and 4 and the IF amplifier after multiplier No. 2, leaving only the difference frequencies. This analog signal processing thus results in conjugate outputs, $A\cos\Phi$ and $A\sin\Phi$; A represents the amplitude/shape of the received ringing and Φ is the phase angle which represents the delay through the EMAT and the electronics plus the elapsed time while propagating in the sample. Both A and Φ are functions of time. These outputs are integrated from several microseconds after the end of the rf burst until no more ringing is observed.

The *amplitude spectrum* of a sample, which is obtained by recording the root of the sum of the squares of the integrator outputs at each frequency, will exhibit sharp peaks at resonance frequencies. Figure 4 presents a resonance line shape from a 6-mm-thick steel sample together with the multiplier outputs $A\cos\Phi$ and $A\sin\Phi$, before integrating, at three frequencies indicated. The ringing signal is made up with the multiple ultrasonic reflections overlapping each other. Phase differences between reflections represent the transit time in the sample. Because the round trip time is an integer multiple of the period at a resonance frequency, all echoes are received in phase only when driving the EMAT at a resonance frequency. Phase Φ is then constant throughout the ring-down time and the integrators give large amplitudes. For slightly off-resonance frequencies, the sample rings down with still large amplitudes because of little interference among echoes. However, Φ changes monotonically and beats appear in the outputs of multiplier Nos. 3 and 4. They tend to integrate to small values, because the changing phase produces both positive and negative outputs. For frequencies far from a resonance, the amplitude decays soon because of destructive interference among reflections. Therefore, two basic mechanisms, the cancellation within the integrator gate and the interference among overlapping echoes, work to make a distinct resonance line shape.

The linewidth of a resonance depends on the attenuation nature of the material, operating parameters, and the sample/EMAT configuration. The choice of operating parameters and EMAT is necessary to obtain an adequate frequency resolution. When a low-loss material is being tested, the integrator gate can be extended enough to attain a thorough cancelling and interference over a large number of echoes. Longer rf bursts produce intense resonances, while they enhance the interference effect with off-resonance frequencies. As for a thick plate, the echo amplitude decays due to diffraction, i.e., the beam spreading, which is characterized by (path length)$\times$(wavelength)/(EMAT diameter)^2.[21] We use a larger EMAT and measure the spectra in a higher frequency range to minimize the diffraction effect. All the operating parameters can be flexibly set in through the attached computer. They include the frequency (every 0.1 Hz in the 0.5–20-MHz range), the rf burst (up to 200 μs long), the amplification factors, the integrator gates, and the number of averaging. This computer also samples the integrator outputs digitized with the 12-bit voltage resolution. Using this analog signal-processing method, a typical measuring time is 10 to 20 s for acquiring and displaying a spectrum, say, with several hundred data points. We fit a symmetric function, e.g., the Gaussian distribution curve, to the discrete spectral data around the peak, whose center axis gives the resonance frequency. The resonance frequency measurements are repeatable typically within the 10-Hz order, or, 10^{-6} frac-

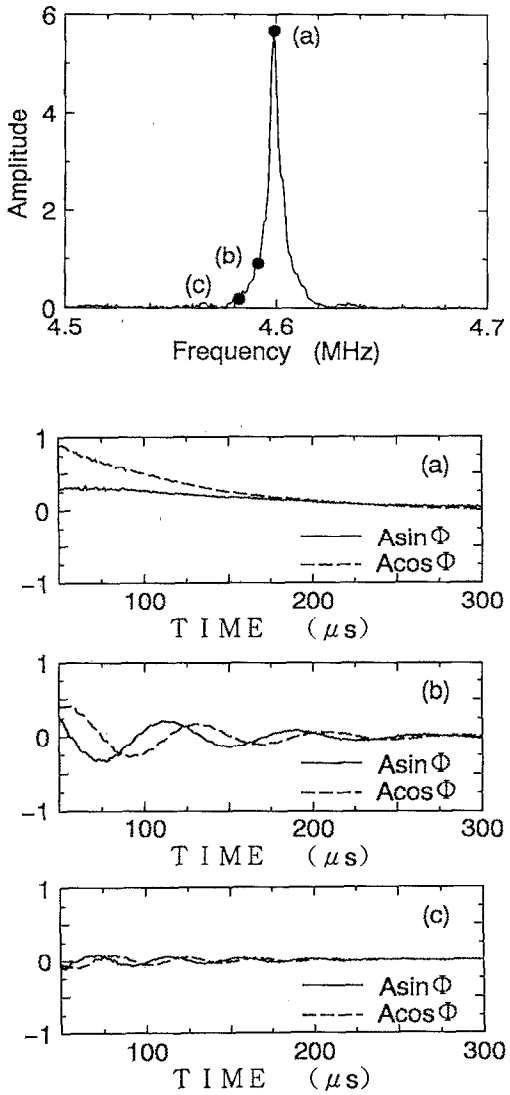

FIG. 4. Resonance line shape and ring-down curves ($A\cos\Phi$ and $A\sin\Phi$) at resonance and off-resonance frequencies.

tional variations. This estimates the ultimate stress resolution as small as 0.1 MPa with the acoustoelastic constants in the order of 10^{-5} MPa^{-1} for common metals.[1]

IV. EXPERIMENTAL RESULTS

A. Acoustoelastic stress measurements

A variety of acoustoelastic stress measurements have been made possible with the above system of resonance EMAT, featuring the noncontacting and high-speed performance. To illustrate the proposed technique, a two-dimensional plane stress field is measured by scanning the EMAT pointwise over the surface of plate samples. We chose thin plate samples, for which conventional time-of-flight methods are incapable of mapping out the stress distribution for the lack of accuracy.

Figure 5 shows the amplitude spectra at two tensile stresses obtained during the calibration tests for the acoustoelastic constants. The dual-mode EMAT was used. The frequency was incremented for the 10.2–10.6-MHz range

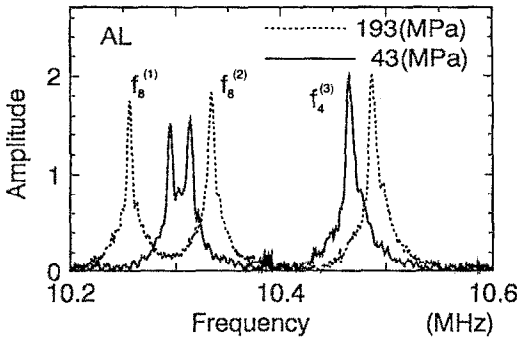

FIG. 5. Acoustoelastic response of resonance curves in uniaxial loading. Sample is 2017 aluminum alloy 1.22-mm thick.

by 800-Hz steps. There are three resonance peaks in this region, corresponding to $f_8^{(1)}$, $f_8^{(2)}$, and $f_4^{(3)}$. The resonance frequencies demonstrate easily detectable changes showing the acoustoelastic phenomena. Two shear-wave peaks for orthogonal polarizations were superimposed over each other in the absence of stress because of very small texture anisotropy. The stress-induced anisotropy made them separate. Both B and R showed the linear dependence on stress as the theory predicts (Fig. 6). We observe that the peak heights also change with stress. This is an open problem at present.

We produced a two-dimensional stress field by stretching an aluminum 2017 strip with a center hole as sketched in Fig. 7. The strip was 1.22-mm thick, 150-mm wide, and 670-mm long. The diameter of the hole was 30 mm. Surface preparation was unnecessary. Since B_0 and R_0 were nearly homogeneous over the scanning area, we used their representative values in calculating stresses; the error is estimated to be less than 2.7 MPa. A typical measurement was done with the 500-V rf bursts of 40-μs duration, approximately 50 times the round-trip time, 34 dB for receiver gain, and the 250-μs long integrator gate. Frequency increment was 600 Hz. Along the Y axis, we scanned the shear-wave EMAT (5×4 mm^2), oriented 45°, to detect B and to depict the variation of the principal stress difference $(\sigma_{xx}-\sigma_{yy})$. σ_{yy} is smaller than a part of a tenth of σ_{xx}. The stress difference was not large enough to resolve the shear-wave polarization on the X axis. We then rotated the above

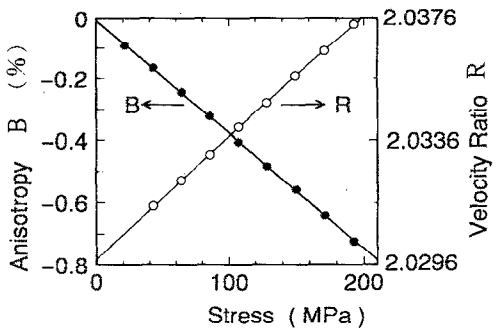

FIG. 6. Linear dependence of B and R on uniaxial stress σ_1 in 2017 aluminum sample; $B_0=0.006\%$ and $C_A=-3.69\times10^{-5}$ MPa^{-1}; $R_0=2.0298$ and $C_R=3.93\times10^{-5}$ MPa^{-1}.

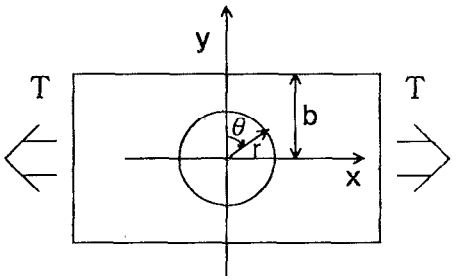

FIG. 7. Strip with a center hole in the plane-stress state.

EMAT to 0°/90° and obtained $f_8^{(1)}$ and $f_8^{(2)}$. The longitudinal resonance frequency was measured using the dual-mode EMAT (10-mm diameter). Their combination results in the separate determination of σ_{xx} and σ_{yy}. We used the calibrated values of C_A and C_R from the uniaxial tests (Fig. 6). The acoustoelastic measurements are compared with Howland's solution[22] in Fig. 8, where the averages on both sides of the hole are presented. The local stress field has been averaged over the EMAT aperture. Such a correction was, however, useless except for the proximity of the edges and the rim. The measurement agrees with the theory within the fluctuation of 5 MPa. Approaching the edges and the rim, the disagreement increases close to 10 MPa. This is attributable to the abrupt variation of stresses within the EMATs' apertures, the inclusion of reflections from the lateral boundaries, and the inhomogeneity of B_0 and R_0 which might be introduced when the hole was drilled.

Along the rim, the stress is not acting in the X and Y axes and B is related to the principal stresses through a more general formula[23]:

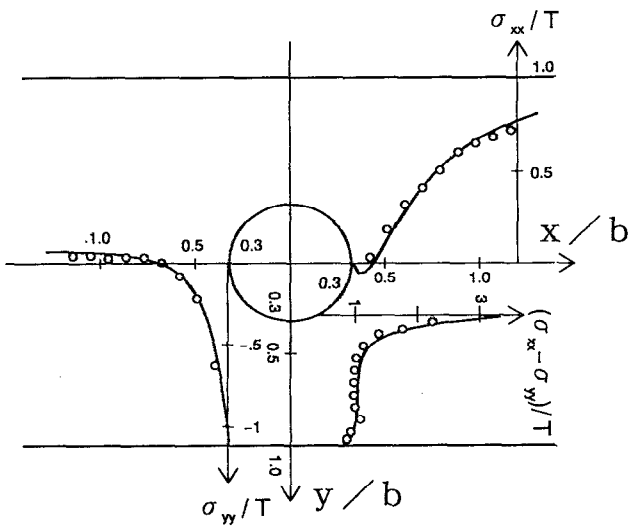

FIG. 8. Stresses around the center hole of stretched strip. Howland's solution is shown in solid curves. Stresses are scaled by the stress at infinity (T=53.5 MPa) and the coordinate by b, half-width of the strip.

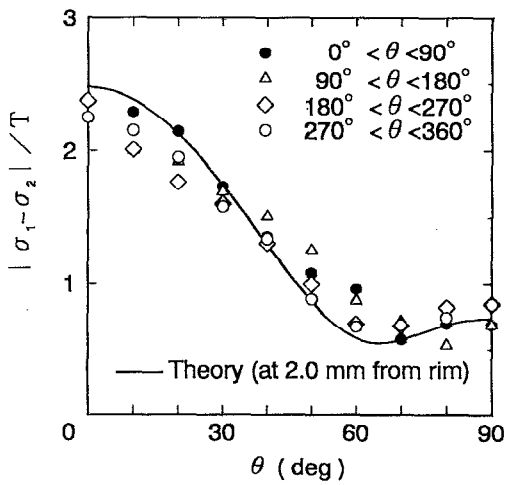

FIG. 9. Comparison between resonance measurement and theory along each quarter of the rim (T=53.5 MPa).

$$B=\frac{f_n^{(1)}-f_n^{(2)}}{(f_n^{(1)}+f_n^{(2)})/2}$$

$$=[B_0^2+2B_0C_A(\sigma_1-\sigma_2)\cos 2\theta+C_A^2(\sigma_1-\sigma_2)^2]^{1/2}, \quad (3)$$

where θ is the angle between the principal direction and the specimen axis. There is only one nonzero principal stress on the rim. We include the radial component, because the EMATs have the finite aperture and the stress field changes steeply in the vicinity of the hole. Figure 9 compares the results of stress measurement using the above shear-wave EMAT to the theory calculated at 2 mm outside the rim, where the center of the EMAT is traced. Disagreement among the quarters could be caused by the slight eccentricity and imperfect roundness of the hole. Maximum error was 15 MPa in this experiment.

B. Effect of liftoff

To examine another aspect of the applicability, we have tested the tolerance to the liftoff using the same aluminum plate and the 10-mm-diam dual-mode EMAT. We inserted polymer sheets to simulate a liftoff between the EMAT and the plate. Figure 10 shows the observed decrease of the peak heights. We swept the frequency every 4 kHz. The input rf voltage and the receiver gain were raised to compensate for the decreasing transduction efficiency with the liftoff; the maximum voltage was 1500 V and the maximum gain was 46 dB. Resonance frequencies were measurable until the liftoff was 2.67 mm and both $f_8^{(1),(2)}$ and $f_4^{(3)}$ decreased by 0.45% and 0.32%, respectively, relative to those for the contacting measurements. Changes in B and R are generally one order less than the frequency changes. Use of EMATs having larger aperture can extend the limiting liftoff and reduce the undesirable shift of resonance frequencies.

V. DISCUSSION

The pulsed ultrasonic resonance spectrometer incorporated with the EMATs has been proven to permit the prac-

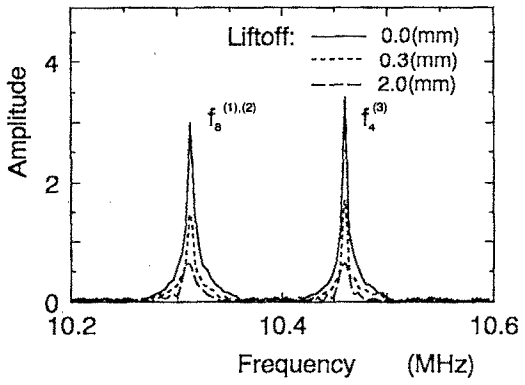

FIG. 10. Appearance of amplitude spectra as a function of increasing liftoff.

tical acoustoelastic stress measurements, showing remarkable frequency and spatial resolutions. A number of mechanisms contribute to realize the high absolute accuracy and reproducibility. They can be sorted as follows: (1) the contactless transduction exerts minimum influence to the elastic wave fields, excluding the distortion which continues to make problems for the mechanical coupling; (2) the heterodyne receiver detects only the driving frequencies and eliminates other frequency components involved; (3) the weak signals by the EMATs further become weaker through their mutual interference for off-resonance frequencies, whereas they pile up to be intense amplitudes only at resonances; and (4) the analog integration makes the most of the small phase change in the received ringing signals at slightly off-resonance conditions and yields highly reduced amplitudes.

Similar stress measurement was possible with ferrous metals.[24,25] But, in general, the signal amplitudes are weaker and the frequency resolution gets worse, especially on austenitic steels. There are two reasons: (1) Steels have larger attenuation coefficients, which can be traced back to the larger elastic anisotropy of constituent single crystals. The anisotropic factor takes the value of 1.22 for aluminum, while it is 2.48 for α-iron and 3.47 for austenitic stainless steel.[26,27] (2) The large magnetic permeability makes the induced current rapidly decay and oscillate along the depth, as is indicated by the solution of Maxwell's equation for a conducting half-space.[6,7,28] Together with the lower conductivity, the eddy current in steels is much smaller than in aluminum alloys; so is the forcing intensity. These two effects are magnified as the frequency increases. But even more, the acoustoelastic constants of steels are several times smaller than aluminum alloys.

The measurable thickness of plate ranges from submillimeter to a few centimeters for most polycrystalline metals. We made the resonance measurements on 0.15-mm-thick aluminum sheets from beverage cans and, using a shear-wave EMAT of 10-mm-square active area, on 34-mm-thick plates of low carbon steel. For thin plates, the resonance frequencies are widely spread. As the thickness decreases, the intervals of the resonances increase and finally the lowest resonance moves out of the frequency band of the EMAT/instrument system. Since the highest frequency of 20 MHz is available, we can detect the resonance in metal sheets of approximately 0.08-mm thick using shear-wave EMATs. The peak separation becomes small, when a thick plate is under test. Overlapping of successive resonance peaks, even partially, reduces the accuracy of the resonance frequency determination. The upper limit of measurable thickness depends on the attenuation character, because it largely determines the width of resonant line shape. We use the larger EMATs to reduce the diffraction in thick plates and choose the parameters to achieve strong resonances.

ACKNOWLEDGMENTS

The authors are indebted to C. M. Fortunko (National Institute of Standards and Technology) and G. L. Petersen (Ritec, Inc.), who participated in the initiating stage of this study. They also thank T. Yamasaki for designing EMATs and valuable discussions on their operation mechanisms. This research was supported in part by Grant-in-Aid No. 03555020 from the Japanese Ministry of Education.

[1] Y. H. Pao, W. Sachse, and H. Fukuoka, *Physical Acoustics*, edited by W. P. Mason and R. N. Thurston (Academic, New York, 1984), Vol. XVII, pp. 61–143.
[2] A. V. Clark, Jr., H. Fukuoka, D. V. Mitrakovic, and J. C. Moulder, Ultrasonics **24**, 281 (1986).
[3] H. Fukuoka, *Solid Mechanics Research for Quantitative Nondestructive Evaluation*, edited by J. D. Achenbach and Y. Rajapakse (Martinus Nijhoff, Dordrecht, 1987), pp. 275–299.
[4] H. Fukuoka, *Proceedings of the 5th International Symposium on Nondestructive Charact. Mater.*, edited by T. Kishi *et al.* (Gordon and Breach, London, 1992), pp. 181–192.
[5] G. Alers and A. Manzanares, *Review of Progress in Quantitative NDE*, edited by D. O. Thompson and D. E. Chimenti (Plenum, New York, 1990), Vol. 9, pp. 1757–1764.
[6] H. M. Frost, *Physical Acoustics*, edited by W. P. Mason and R. N. Thurston (Academic, New York, 1979), Vol. XIV, pp. 179–276.
[7] R. B. Thompson, *Physical Acoustics*, edited by R. N. Thurston and A. D. Pierce (Academic, New York, 1988), Vol. XIX, pp. 157–200.
[8] B. W. Maxfield and C. M. Fortunko, Mater. Eval. **41**, 1399 (1983).
[9] B. I. Bolef and M. J. Menes, J. Appl. Phys. **31**, 1010 (1960).
[10] G. Mozurkewich, J. Acoust. Soc. Am. **86**, 885 (1989).
[11] M. Hirao, H. Fukuoka, and Y. Murakami, Res. Nondestr. Eval. **4**, 127 (1992).
[12] S. A. Filimonov, B. A. Budenko, and N. A. Glukhov, Sov. J. Nondestr. Test. **1**, 102 (1971).
[13] Z. G. Nikiforenko, N. A. Glukhov, and I. I. Averbukh, Sov. J. Nondestr. Test. **4**, 427 (1971).
[14] K. Kawashima, J. Acoust. Soc. Am. **87**, 681 (1990).
[15] W. L. Johnson, S. J. Norton, F. Bendic, and R. Pless, J. Acoust. Soc. Am. **91**, 2637 (1992).
[16] A. V. Clark, Jr., C. M. Fortunko, M. G. Lozev, S. R. Schaps, and M. C. Renken, Res. Nondestr. Eval. **4**, 165 (1992).
[17] K. Kawashima, J. Acoust. Soc. Am. **60**, 365 (1976).
[18] C. M. Fortunko, G. L. Petersen, B. B. Chick, M. C. Renken, and A. L. Preis, Rev. Sci. Instrum. **63**, 3477 (1992).
[19] G. L. Petersen, B. B. Chick, and C. M. Fortunko, *Proceedings of the 5th International Symposium on Nondestructive Charact. Mater.*, edited by T. Kishi *et al.* (Gordon and Breach, London, 1992), pp. 847–856.
[20] G. L. Petersen, C. M. Fortunko, M. Hirao, and B. B. Chick, Rev. Sci. Instrum. **65**, Jan (1994).
[21] H. Seki, A. Granato, and R. Truell, J. Acoust. Soc. Am. **28**, 230 (1956).
[22] R. C. J. Howland, Philos. Trans. R. Soc. London Ser. A **229**, 49 (1930).
[23] Y. Iwashimizu and K. Kubomura, Int. J. Solids Struct. **9**, 99 (1973).

[24] H. Fukuoka, M. Hirao, T. Yamasaki, H. Ogi, G. L. Petersen, and C. M. Fortunko, *Review of Progress in Quantitative NDE*, edited by D. O. Thompson and D. E. Chimenti (Plenum, New York, 1993), Vol. 12, pp. 2129–2136.
[25] M. Hirao, H. Ogi, T. Yamasaki, and H. Fukuoka, *Proceedings of the 6th International Symposium on Nondestructive Charact. Mater. (Hawaii)*, edited by R. E. Green, Jr. *et al.* (Plenum, New York, 1993).
[26] M. J. P. Musgrave, *Crystal Acoustics* (Holden Day, San Francisco, 1970).
[27] D. S. Kupperman and K. J. Reimann, IEEE Trans. Sonics Ultrason. SU-27, 7 (1980).
[28] J. D. Jackson, *Classical Electrodynamics* (Wiley, New York, 1962).